

Mapping the composition-dependence of the energy bandgap of GaAsNBi alloys

Cite as: Appl. Phys. Lett. **115**, 082106 (2019); <https://doi.org/10.1063/1.5057424>

Submitted: 14 September 2018 . Accepted: 21 July 2019 . Published Online: 23 August 2019

J. Occena , T. Jen , J. W. Mitchell, W. M. Linhart , E.-M. Pavelescu, R. Kudrawiec , Y. Q. Wang, and R. S. Goldman 



View Online



Export Citation



CrossMark

ARTICLES YOU MAY BE INTERESTED IN

[InAsSb-based heterostructures for infrared light modulation](#)

Applied Physics Letters **115**, 081102 (2019); <https://doi.org/10.1063/1.5111980>

[Ultra-wide-bandgap AlGaN homojunction tunnel diodes with negative differential resistance](#)

Applied Physics Letters **115**, 082104 (2019); <https://doi.org/10.1063/1.5113503>

[Limitations of In₂O₃ as a transparent conducting oxide](#)

Applied Physics Letters **115**, 082105 (2019); <https://doi.org/10.1063/1.5109569>



Instruments for Advanced Science

Contact Hiden Analytical for further details:
www.HidenAnalytical.com
info@hiden.co.uk

[CLICK TO VIEW](#) our product catalogue



Gas Analysis

- dynamic measurement of reaction gas streams
- catalysis and thermal analysis
- molecular beam studies
- dissolved species probes
- fermentation, environmental and ecological studies



Surface Science

- UHV/TPD
- SIMS
- end point detection in ion beam etch
- elemental imaging - surface mapping



Plasma Diagnostics

- plasma source characterization
- etch and deposition process reaction kinetic studies
- analysis of neutral and radical species



Vacuum Analysis

- partial pressure measurement and control of process gases
- reactive sputter process control
- vacuum diagnostics
- vacuum coating process monitoring

Mapping the composition-dependence of the energy bandgap of GaAsN_xBi_y alloys

Cite as: Appl. Phys. Lett. **115**, 082106 (2019); doi: [10.1063/1.5057424](https://doi.org/10.1063/1.5057424)

Submitted: 14 September 2018 · Accepted: 21 July 2019 ·

Published Online: 23 August 2019



View Online



Export Citation



CrossMark

J. Occena,¹ T. Jen,¹ J. W. Mitchell,¹ W. M. Linhart,² E.-M. Pavelescu,³ R. Kudrawiec,² Y. Q. Wang,⁴ and R. S. Goldman^{1,a)}

AFFILIATIONS

¹Department of Materials Science and Engineering, University of Michigan, Ann Arbor, Michigan 48109-2136, USA

²Faculty of Fundamental Problems of Technology, Wrocław University of Science and Technology, 50-370 Wrocław, Poland

³National Institute for Research and Development in Microtechnologies, 077190 Bucharest, Romania and Hyperion University, 030615 Bucharest, Romania

⁴Materials Science and Technology Division, Los Alamos National Laboratory, Los Alamos, New Mexico 87545, USA

^{a)}Author to whom correspondence should be addressed: rsgold@umich.edu

ABSTRACT

We have examined the alloy composition dependence of the energy bandgap and electronic states in GaAsN_xBi_y alloys. Using direct measurements of N and Bi mole fractions, via ion beam analysis, in conjunction with direct measurements of the out-of-plane misfit via x-ray rocking curves, we determine the “magic ratio” for lattice-matching of GaAsN_xBi_y alloys with GaAs substrates. In addition, using a combination of photoreflectance and photoluminescence spectroscopy, we map the composition- and misfit-dependence of the energy bandgaps, along with revealing the energetic position of Bi-related states at approximately 0.18 eV above the valence band maximum.

Published under license by AIP Publishing. <https://doi.org/10.1063/1.5057424>

Due to the significant bandgap narrowing induced by the incorporation of dilute fractions of N and Bi into compound semiconductors, emerging dilute nitride-bismide alloys are of significant interest for optoelectronic devices operating in the near- to mid-infrared range.^{1,2} In the literature, the magic N to Bi mole fraction ratio for lattice matching of GaAsN_xBi_y with GaAs is predicted to be equal to 0.59, based upon a computed value of the GaBi lattice parameter.¹ In addition, the relationship between the composition and the bandgap value is most often determined using x-ray diffraction measurements of strain to determine the alloy composition, assuming the computed value of the GaBi lattice parameter, with films fully strained to the GaAs substrate. For GaAsN_xBi_y, it has recently been shown that Bi promotes the formation of (N-As)_{As} interstitial complexes,³ which are not accounted for in typical analyses of x-ray diffraction data. Furthermore, it has been proposed that Bi behaves as an isoelectronic impurity in GaAs. However, there are conflicting reports regarding the energetic position of the Bi impurity state either 0.18 eV above¹ or 0.08–0.4 eV below^{4–9} the valence band maximum.

Here, we use a combination of direct measurements of alloy compositions, via ion beam analyses of the N and Bi mole fractions, direct measurements of the out-of-plane misfit using high-resolution x-ray diffraction, and measurements of the bandgap using photoreflectance (PR), to determine a N/Bi ratio for lattice-matching and a map of the

composition dependence of GaAsN_xBi_y bandgaps. Furthermore, a comparison of PR and photoluminescence (PL) spectra reveals the presence of a Bi-related state ~0.18 eV above the valence band edge, consistent with the predictions of Janotti *et al.*¹ These findings offer a predictive guide to bandgap engineering using GaAsN_xBi_y alloys and provide insight into the combined influence of Bi and N on electronic structure that may be extended to other emerging dilute nitride-bismide alloys, such as GaPN_xBi_y and InAsN_xBi_y.

A series of GaAs_{1-x-y}N_xBi_y films were grown by molecular-beam epitaxy, as described elsewhere.^{3,10} A range of N and Bi fractions were achieved by varying the N₂ flow rate from 0 to 0.35 sccm (N flux series) and the Bi beam-equivalent pressure (BEP) from 0 to 1.2×10^{-7} Torr (Bi flux series). Films with 100 nm (“thin”) and 400 nm (“thick”) thicknesses were prepared. High-resolution x-ray diffraction measurements were performed using a Bede D1 and/or Rigaku Smartlab diffractometer with CuK α_1 radiation monochromated by two Si channel cut crystals, consisting of (220) reflections in the duMond-Hart-Bartels (+, -, -, +) configuration. X-ray rocking curves (XRCs) were collected near the (004) and (224) GaAs reflections. The out-of-plane misfit was determined directly from the (004) XRCs as

$$\varepsilon_{\perp} = \frac{\sin(\theta_B)}{\sin(\theta_B + \Delta\omega)} - 1, \quad (1)$$

where θ_B is the (004) GaAs Bragg angle and $\Delta\omega$ is the peak splitting between the film and the GaAs substrate (004) reflections.¹¹ The in-plane misfit was determined from an analysis of glancing-incidence (224) XRCs; the misfit and residual in-plane strain were then computed assuming a tetragonally distorted lattice with the Poisson ratio of GaAs, as described in the [supplementary material](#). The resulting misfit values range from -0.16% to 0.46% . According to Refs. 12–14, the critical thickness for dislocation nucleation is expected to exceed 200 nm. Thus, the thin films are expected to be coherently strained, consistent with the negligible strain relaxation computed using XRC, as shown in Table S1 of the [supplementary material](#). For the thick films which contain Bi, negligible strain relaxation is also observed, suggesting that they are also coherently strained. However, the thick film without Bi is partially (14%) relaxed, presumably due to the nucleation of 90° partial dislocations whose misfit component is nearly double that of 60° dislocations.¹⁵ Indeed, 90° partial dislocations have been observed in tensile-strained films such as GaAsN.¹⁶ If we attribute the (004) XRC linewidths for the Bi-containing thick films (52.5 ± 2.5 arcseconds) to 60° dislocations and that of the Bi-free thick film (60 arcseconds) to 90° partial dislocations, the resulting dislocation densities would be $\sim 5 \times 10^5 \text{ cm}^{-2}$ and $2 \times 10^6 \text{ cm}^{-2}$, consistent with the differences in the measured strain relaxation. In this case, the lack of appreciable strain relaxation in the Bi-containing tensile strained thick film is likely due to the surfactant action of Bi suppressing the formation of 90° partial dislocations.

For all films, the Bi fractions were determined using Rutherford backscattering spectrometry (RBS), in conjunction with simulation of nuclear reaction analysis (SIMNRA) code, as described elsewhere.^{3,17} For the thin films, the total, substitutional, and interstitial N fractions were determined using channeling nuclear reaction analysis (NRA), also in conjunction with SIMNRA code. In addition, for all films, the Bi fractions from RBS and the nominal film thicknesses were used as input into dynamical diffraction simulations via the Rocking-Curve Analysis using Dynamical Simulations (RADS) software. Interestingly, the RADS-determined N fractions were consistent with the substitutional N fraction determined using NRA, which is typically 75% of the total N fraction determined using NRA, consistent with the trends reported elsewhere.^{3,15} Therefore, to take into account the interstitials in the thick films, the total N fraction was determined as the RADS N fraction (substitutional fraction) divided by 0.75.^{3,18}

To measure the PR spectra, each sample was mounted on a cold finger in a helium closed cycle refrigerator coupled with a programmable temperature controller, allowing measurements in the 20–320 K temperature range. The reflected light from the sample was dispersed by a single grating 0.55 m focal-length monochromator and detected using a thermoelectrically cooled InGaAs p-i-n photodiode. To illuminate the sample, a semiconductor laser (532 nm line) and a 150 W tungsten-halogen bulb were used as the pump and probe beams, respectively, which were focused onto the sample to a diameter of ~ 2 mm. The pump beam was modulated by a mechanical chopper at a frequency of 290 Hz. Phase sensitive detection of the PR signal was made using a lock-in amplifier. PL spectra were collected using a continuous-wave laser with a wavelength of 532 nm and excitation powers of 100 or 300 mW.

In Fig. 1, contours of out-of-plane misfit are presented on a plot of Bi vs N fraction for $\text{GaAs}_{1-x-y}\text{N}_x\text{Bi}_y$ films with circular and square symbols corresponding to 100 nm and 400 nm thick films, respectively.

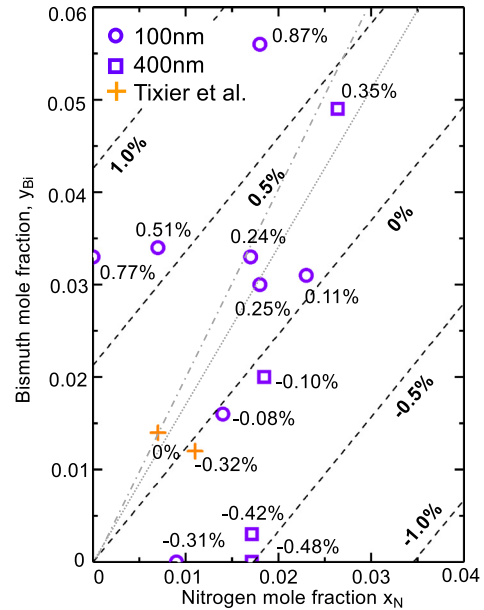


FIG. 1. Contours of the out-of-plane misfit, ε_{\perp} , presented on a plot of bismuth mole fraction, y_{Bi} , and nitrogen mole fraction, x_{N} , for $\text{GaAs}_{1-x-y}\text{N}_x\text{Bi}_y$ films; circular and square symbols correspond to 100 nm and 400 nm thick films, respectively. The percent out-of-plane misfit, ε_{\perp} , determined from (004) XRC, is labeled adjacent to each point. Dashed black lines represent the contours of constant misfit, determined with a planar fit to the data points, indicating lattice-matching for a N to Bi mole fraction ratio of 0.83. Lattice-matched N to Bi mole fraction ratios of 0.59 computed by Janotti *et al.*¹ and 0.49 estimated from x-ray diffraction determinations of the N mole fraction by Huang *et al.*¹⁹ are shown by gray lines. Cross symbols represent the GaAsNBi films from Ref. 21. The uncertainty in the ε_{\perp} contour lines is $\pm 0.04\%$, defined as the standard deviation between the fit and measured values of ε_{\perp} .

For each composition, the out-of-plane misfit, ε_{\perp} , determined from (004) x-ray rocking curves, as described in Eq. (1), is labeled near each point. Using a planar fit to the data points represented by circular symbols, with $R^2 = 0.97$, contours of constant ε_{\perp} , indicated by dashed black lines, reveal a N to Bi mole fraction ratio for the lattice-matching of 0.83. For comparison, the predicted lattice-matched N to Bi mole fraction ratios of 0.59 from the study by Janotti *et al.*¹ and 0.49 estimated using x-ray diffraction determinations of the N fraction by Huang *et al.*¹⁹ are shown by gray lines. We note that a non-negligible fraction of N in GaAsNBi has been reported to be incorporated interstitially,^{3,20} predominantly in the form of $(\text{N-As})_{\text{As}}$ complexes, which are not accounted for in Janotti's calculations and the x-ray diffraction determinations of the N fraction by Huang *et al.*¹⁹ and Tixier *et al.*²¹ Indeed, a planar fit to ε_{\perp} , using the substitutional N fraction, rather than the total N fraction, yields a lattice-matched N to Bi mole fraction ratio of 0.61, in agreement with the predictions of Janotti *et al.*¹

We now consider the optical properties of the N flux series and Bi flux series of GaAsNBi alloys, as shown in the low-temperature (i.e., $T = 20$ K) PR spectra shown in Figs. 2(a) and 2(b), respectively. For each PR spectrum, features that are attributed to energy transitions, i.e., resonances, are apparent. To determine the energy, E_0 , of each transition and its broadening, the PR spectra were fitted using the Aspnes formula²²

$$\frac{dR}{R}(E) = \text{Re}[Ce^{i\theta}(E - E_0 + i\Gamma)^{-m}], \quad (2)$$

where $\frac{dR}{R}(E)$ is the energy dependence of the PR signal, C and θ denote the amplitude and phase, and E_0 and Γ are the energy and the broadening parameter of the optical transition, respectively. Assuming $m = 2$ for an excitonic transition, we fit each spectrum with a low and high energy resonance, shown as black and red vertical dashed lines in the plots in Fig. 2. For each resonance, further visualization of the transition energies is enabled by plots of the moduli of the PR resonances, 23 shown as gray dashed lines in Fig. 2,

$$\Delta\rho(E) = \frac{|C|}{[(E - E_0)^2 + \Gamma^2]^{\frac{m}{2}}}. \quad (3)$$

With the increasing N fraction and/or Bi fraction, there is a monotonic decrease, i.e., a redshift, of the bandgap to lower energies. For some spectra, a second resonance is apparent at slightly higher energy than the bandgap, likely due to strain-induced splitting of the light-hole and heavy-hole bands.²³ For other spectra, the broadening of the PR resonances and the small degree of splitting make it difficult to resolve the second transition. In all cases, the bandgap energy, E_g , is determined as the sum of the excitonic transition (determined from the low-energy PR resonance) plus the exciton binding energy (~ 8 meV), taking into account strain-induced shifts of the band-edges at the measurement temperature (~ 20 K).

In Fig. 3, contours of the bandgap and out-of-plane misfit are presented on a plot of Bi vs N mole fractions for $\text{GaAs}_{1-x-y}\text{N}_x\text{Bi}_y$ films. Dashed black lines indicate the contours of constant out-of-plane misfit, while circular and square symbols represent individual GaAsNBi films, as described in Fig. 1. Bandgaps measured by PR for specific films are labeled besides each data point. Solid contours indicate the composition-dependence of the bandgap energy (in electron-volt), E_{GaAsNBi} , determined by fitting the measured bandgaps and compositions using the parameterization scheme reported by Tixier *et al.*,²¹

$$E_{\text{GaAsNBi}}(x_N, y_{\text{Bi}}) = E_{\text{GaAs}} - \Delta_N(x_N) - \Delta_{\text{Bi}}(y_{\text{Bi}}) - A\Delta_N(x_N)\Delta_{\text{Bi}}(y_{\text{Bi}}), \quad (4)$$

where E_{GaAs} is the bandgap of GaAs at 20 K, $\Delta_N(x_N)$ is the N-induced bandgap reduction in GaAsN, $\Delta_{\text{Bi}}(y_{\text{Bi}})$ is the Bi-induced bandgap reduction in GaAsBi, and A is an adjustable N-Bi coupling parameter. The N-induced bandgap reduction (in electron-volt) is expressed as

$$\Delta_N(x_N) = x_N(E_{\text{GaAs}} - E_{\text{GaAsN}}) + b_{\text{GaAsN}}x_N(1 - x_N), \quad (5)$$

where E_{GaAsN} is the bandgap of GaN and b_{GaAsN} is the bowing parameter (in electron-volt) with a double-exponential dependence on the N fraction,^{24,25}

$$b_{\text{GaAsN}}(x_N) = 9.4 + 23.8e^{-x_N/0.0038} + 11.9e^{-x_N/0.028}. \quad (6)$$

The double-exponential dependence of the bowing parameter on x_N has been attributed to three regimes of bandgap energy, which are dominated by single-impurity N levels, N pair and cluster states, and alloy behavior, respectively.^{25–27} To estimate the Bi-induced bandgap reduction, we used our PR determination of the GaAsBi bandgap as $\Delta_{\text{Bi}}(y_{\text{Bi}}) = 7.3 y_{\text{Bi}}$ (in electron-volt), which is similar to the average value of 7.8 y_{Bi} from earlier reports.^{7,19,28–30} Using a nonlinear least squares fit to

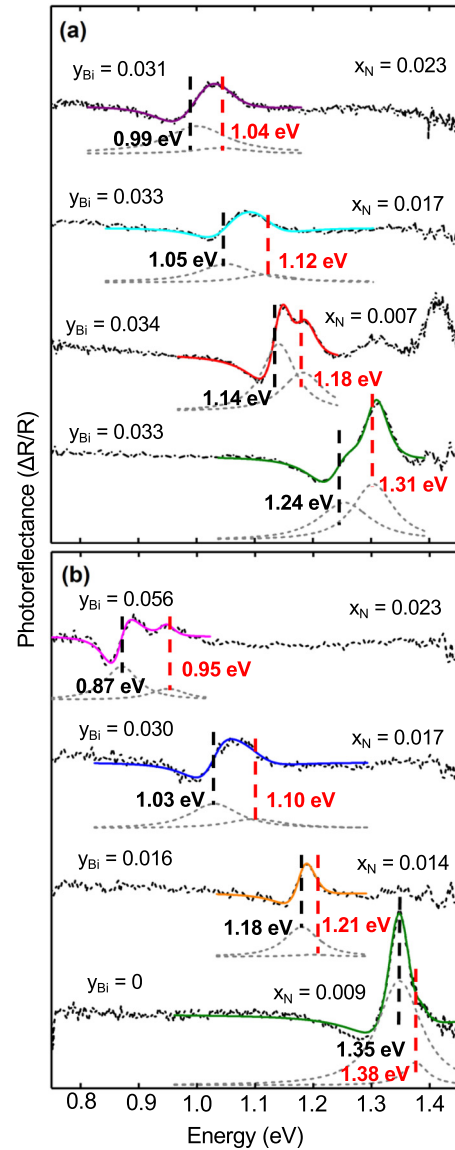


FIG. 2. Photoreflectance (PR) spectra collected at 20 K from 100 nm thick $\text{GaAs}_{1-x-y}\text{N}_x\text{Bi}_y$ films, with corresponding N and Bi mole fractions, x_N and y_{Bi} , displayed above each spectrum for (a) the N flux series and (b) the Bi flux series. For each spectrum, PR resonance attributed to the bandgap energy, E_g , is indicated by a black dashed line. With increasing x_N and/or y_{Bi} , the E_g values decrease monotonically. For some spectra, a second transition, attributed to strain-induced splitting of the light-hole and heavy-hole bands, is indicated by a red vertical dashed line. The energy of each resonance was determined by fitting each spectrum with the Aspnes formula²⁰ (solid lines). The moduli of the PR resonances are shown as gray dashed lines below each PR spectrum.

Eq. (4),^{31,32} the N-Bi coupling parameter $A = -0.02 \pm 0.10 \text{ eV}^{-1}$, which corresponds to a value of $-(1-2)$ meV for the final term in Eq. (4). Thus, the quaternary bandgap reduction is essentially the sum of the individual bandgap reductions, suggesting that N and Bi independently influence the band edges, as predicted by Broderick *et al.*,⁷ but in contrast to earlier reports that indicate nonzero values of A ,^{1,21} which

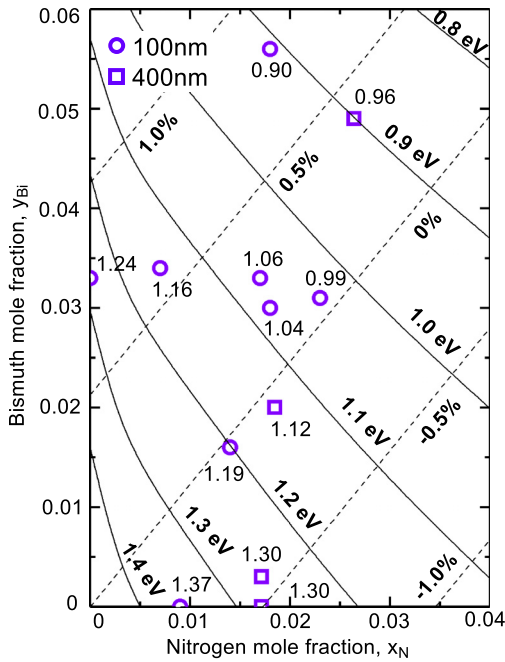


FIG. 3. Contours of bandgap energies, E_g , and out-of-plane misfit, ϵ_{\perp} , presented on a plot of bismuth mole fraction, y_{Bi} , and nitrogen mole fraction, x_{N} , for $\text{GaAs}_{1-x-y}\text{N}_x\text{Bi}_y$ films. The values of E_g determined from photoreflectance spectra collected at 20 K are labeled adjacent to each point. Solid lines of constant E_g were determined by a nonlinear least squares fit of Eq. (4) to the data points. Dashed lines of constant ϵ_{\perp} are determined as described in Fig. 1, with lattice-matching to GaAs at a N to Bi mole fraction ratio of 0.83. The uncertainty in the E_g contour lines is ± 14 meV, defined as the standard deviation between the fit and the measured values of E_g .

correspond to additional bandgap reductions of <20 meV (Ref. 1) and <100 meV.²¹

We next examine PL spectra for a selection of $\text{GaAs}_{1-x-y}\text{N}_x\text{Bi}_y$ films with PR spectra shown in Fig. 2. In Fig. 4(a), PL spectra for a film with $x_{\text{N}} = 0.007$ and $y_{\text{Bi}} = 0.034$ are plotted for measurement temperatures ranging from 7 K to 125 K. With increasing measurement temperature, the PL peak energy decreases monotonically. In addition, above 120 K, the PL intensity decreases, and the emission line shape is asymmetric with an extended low-energy tail,^{33,34} often associated with localized states. These features are typical for dilute nitride and bismide films grown at temperatures lower than those for the GaAs host. However, the narrow PR resonances and VB splitting into heavy and light hole bands suggest high quality, homogeneous alloy films. In Fig. 4(b), the PL peak energies as a function of measurement temperature are compared with the bandgap energy of the film determined from PR measurements collected at 20 K. A solid black line shows a projection of the bandgap to high temperatures using the Varshni model,³⁵

$$E(T) = E(0) - \frac{\alpha T^2}{(T + \beta)}, \quad (7)$$

using the parameters for GaAs ($\alpha = 5.41 \times 10^{-4}$ meV/K; $\beta = 204$ K).³⁶ The ~ 160 meV difference between the PR-determined bandgap, E_{PR} , and the PL-determined energy gap, E_{PL} , i.e., the Stokes shift, suggests emission from localized states.

To examine the origins of the localized state emission, in Fig. 5, we consider PL spectra for several films from (a) the N flux series and

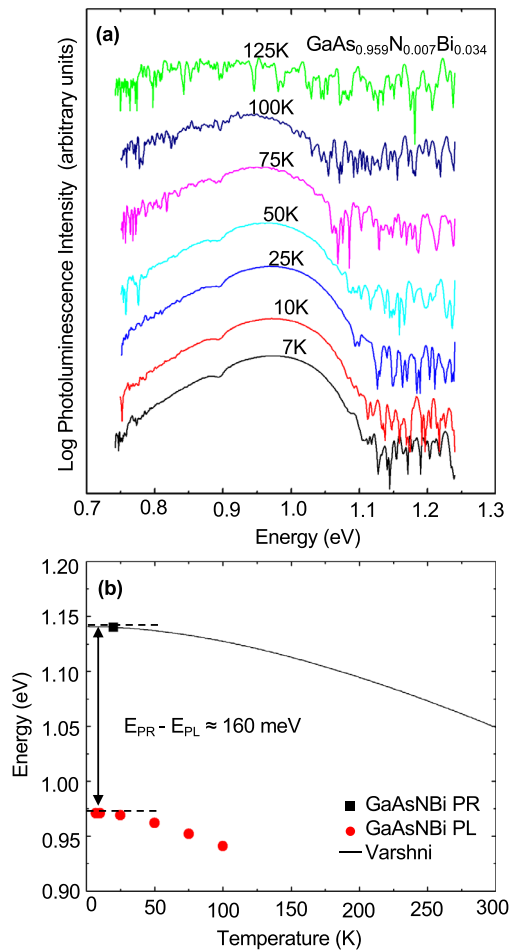


FIG. 4. (a) Photoluminescence PL spectra collected from a $\text{GaAs}_{0.959}\text{N}_{0.007}\text{Bi}_{0.034}$ film at measurement temperatures ranging from 7 to 125 K. The N and Bi mole fractions are listed as x_{N} and y_{Bi} . With the increasing measurement temperature, the PL peak energy decreases monotonically. (b) PL peak energy vs measurement temperature, compared to photoreflectance (PR)-determined bandgap energy, E_g , at 20 K. A solid black line shows a projection of E_g to high temperatures using the Varshni model³⁵ with the parameters for GaAs.³⁶

(b) the Bi flux series. For all Bi-containing films, the Stokes shifts range from 0.15 to 0.18 eV. In contrast, for GaAsN films (i.e., $y_{\text{Bi}} = 0$) in Figs. 5(b) and S1, the differences between E_{PL} and E_{PR} are <60 meV. Taken together, these results suggest that the 7 K PL emission is dominated by an optical transition involving a Bi-related state within the bandgap, approximately 0.18 eV above the valence band edge. Interestingly, Janotti *et al.* predicted a Bi-induced isovalent defect level at 0.18 eV above the valence band edge of GaAsN_{Bi}.¹ Further work is needed to resolve the atomistic origins of the Bi-related states.

In summary, we have examined the alloy composition-dependence of the energy bandgap and lattice misfit in GaAsN_{Bi} alloys. Using direct measurements of N and Bi mole fractions and out-of-plane misfit, we identify a N to Bi mole fraction ratio of 0.83 for lattice-matching to GaAs. Using the substitutional N mole fraction, without including the interstitial N, the lattice-matched N to Bi mole fraction ratio becomes 0.61, in agreement with the predictions of

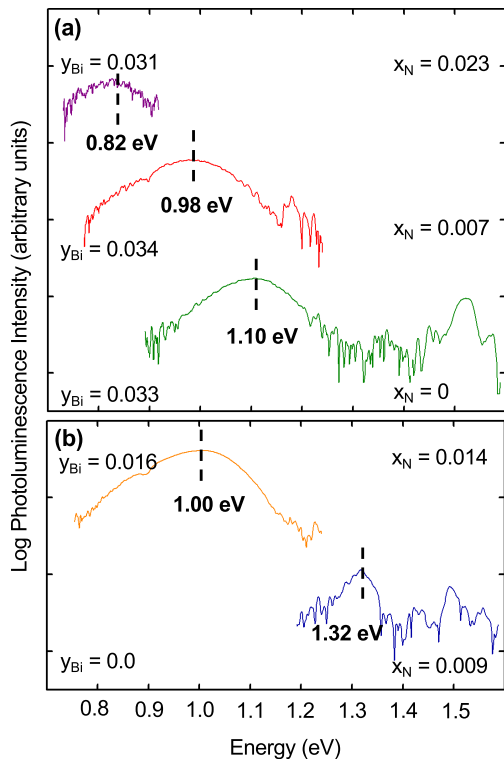


FIG. 5. Photoluminescence (PL) spectra collected at 7K for the selected $\text{GaAs}_{1-x}\text{N}_x\text{Bi}_y$ films whose photoreflectance spectra are shown in Fig. 2. A comparison of the PL-determined peak energies, E_{PL} , with the PR-determined bandgap energies, E_{PR} , in Fig. 2 reveals similar values for the GaAsN film. For the GaAsNBi films, the difference between E_{PR} and E_{PL} , i.e., the Stokes shift, ranges from 0.15 to 0.18 eV, likely due to Bi-related states within the bandgap.

Janotti *et al.*¹ In addition, a comparison of photoreflectance and photoluminescence measurements suggests the presence of Bi-related states ~ 0.18 eV above the valence band edge. These findings offer a predictive guide for bandgap engineering using GaAsNBi alloys and provide insight into the combined influence of Bi and N on the electronic structure that is likely to extend to other emerging dilute nitride-bismide alloys, such as GaPNBi and InAsNBi.

See the [supplementary material](#) for the details of our x-ray rocking curve analysis to determine in-plane strain and its impact on the conduction and valence band edges. In addition, the tabulated values of strain and other parameters used to fit the photoreflectance (PR) spectra, as well as PR spectra for the 400 nm thick films, are included.

We gratefully acknowledge support from the National Science Foundation (Grant Nos. DMR 1410282 and DMR 1810280) and the U. S. Department of Energy Office of Science Graduate Student Research Program. Partial support is also provided by the Center for Integrated Nanotechnologies (CINT), a DOE nanoscience user facility jointly operated by Los Alamos and Sandia National Laboratories. W. M. Linhart acknowledges support from the Polish National Science Center Grant No. 2014/13/D/ST3/01947. This work was partly

supported by a grant from the Ministry of Research and Innovation, CNCS-UEFISCDI, Project No. PN-III-P4-ID-PCE-2016-0742, within PNCDI III.

REFERENCES

- 1A. Janotti, S.-H. Wei, and S. B. Zhang, *Phys. Rev. B* **65**, 115203 (2002).
- 2S. J. Sweeney and S. R. Jin, *J. Appl. Phys.* **113**, 043110 (2013).
- 3J. Occena, T. Jen, E. E. Rizzi, T. M. Johnson, J. Horwath, Y. Q. Wang, and R. S. Goldman, *Appl. Phys. Lett.* **110**, 242102 (2017).
- 4Y. Zhang, A. Mascarenhas, and L.-W. Wang, *Phys. Rev. B* **71**, 155201 (2005).
- 5S. Francoeur, S. Tixier, E. Young, T. Tiedje, and A. Mascarenhas, *Phys. Rev. B* **77**, 085209 (2008).
- 6K. Alberi, O. D. Dubon, W. Walukiewicz, K. M. Yu, K. Bertulis, and A. Krotkus, *Appl. Phys. Lett.* **91**, 051909 (2007).
- 7C. A. Broderick, M. Usman, and E. P. O'Reilly, *Semicond. Sci. Technol.* **28**, 125025 (2013).
- 8C.-Z. Zhao, H.-Y. Ren, T. Wei, S.-S. Wang, and K.-Q. Lu, *J. Electron. Mater.* **47**, 4539 (2018).
- 9V. Virkkala, V. Havu, F. Tuomisto, and M. J. Puska, *Phys. Rev. B* **88**, 235201 (2013).
- 10J. Occena, T. Jen, H. Lu, B. A. Carter, T. S. Jimson, A. G. Norman, and R. S. Goldman, *Appl. Phys. Lett.* **113**, 211602 (2018).
- 11R. S. Goldman, H. H. Wieder, and K. L. Kavanagh, *Appl. Phys. Lett.* **67**, 344 (1995).
- 12J. W. Matthews and A. E. Blakeslee, *J. Cryst. Growth* **27**, 118 (1974).
- 13R. People and J. C. Bean, *Appl. Phys. Lett.* **47**, 322 (1985).
- 14P. M. J. Marea, J. C. Barbour, J. F. Van der Veen, K. L. Kavanagh, C. W. T. Bulle-Lieuwma, and M. P. A. Vieggers, *J. Appl. Phys.* **62**, 4413 (1987).
- 15R. S. Goldman, K. L. Kavanagh, H. H. Wieder, S. N. Ehrlich, and R. M. Feenstra, *J. Appl. Phys.* **83**, 5137 (1998).
- 16M. Reason, X. Weng, W. Ye, D. Dettling, S. Hanson, G. Obeidi, and R. S. Goldman, *J. Appl. Phys.* **97**, 103523 (2005).
- 17T. Jen, G. Vardar, Y. Q. Wang, and R. S. Goldman, *Appl. Phys. Lett.* **107**, 221904 (2015).
- 18M. Reason, H. A. McKay, W. Ye, S. Hanson, R. S. Goldman, and V. Rotberg, *Appl. Phys. Lett.* **85**, 1692 (2004).
- 19W. Huang, K. Oe, G. Feng, and M. Yoshimoto, *J. Appl. Phys.* **98**, 053505 (2005).
- 20P. Wei, S. Tixier, M. Chicoine, S. Francoeur, A. Mascarenhas, T. Tiedje, and F. Schiettekatte, *Nucl. Instrum. Methods Phys. Res., Sect. B* **219–220**, 671 (2004).
- 21S. Tixier, S. E. Webster, E. C. Young, T. Tiedje, S. Francoeur, A. Mascarenhas, P. Wei, and F. Schiettekatte, *Appl. Phys. Lett.* **86**, 112113 (2005).
- 22D. E. Aspnes, *Surf. Sci.* **37**, 418 (1973).
- 23R. Kudrawiec and J. Misiewicz, in *Semiconductor Research*, edited by A. Patane and N. Balkan (Springer Berlin Heidelberg, Berlin, Heidelberg, 2012), pp. 95–124.
- 24M. Reason, Ph.D. thesis, University of Michigan, 2006.
- 25U. Tisch, E. Finkman, and J. Salzman, *Appl. Phys. Lett.* **81**, 463 (2002).
- 26P. R. C. Kent and A. Zunger, *Phys. Rev. B* **64**, 115208 (2001).
- 27R. L. Field, Y. Jin, H. Cheng, T. Dannecker, R. Jock, Y. Wang, C. Kurdak, and R. S. Goldman, *Phys. Rev. B* **87**, 155303 (2013).
- 28S. Tixier, M. Adamczyk, T. Tiedje, S. Francoeur, A. Mascarenhas, P. Wei, and F. Schiettekatte, *Appl. Phys. Lett.* **82**, 2245 (2003).
- 29S. Francoeur, M. J. Seong, A. Mascarenhas, S. Tixier, M. Adamczyk, and T. Tiedje, *Appl. Phys. Lett.* **82**, 3874 (2003).
- 30A. R. Mohmad, F. Bastiman, J. S. Ng, S. J. Sweeney, and J. P. R. David, *Phys. Status Solidi C* **9**, 259 (2012).
- 31K. Levenberg, *Q. Appl. Math.* **2**, 164 (1944).
- 32D. Marquardt, *J. Soc. Ind. Appl. Math.* **11**, 431 (1963).
- 33S. Imhof, A. Thranhardt, A. Chernikov, M. Koch, N. S. Köster, K. Kolata, S. Chatterjee, S. W. Koch, X. Lu, S. R. Johnson, D. A. Beaton, T. Tiedje, and O. Rubel, *Appl. Phys. Lett.* **96**, 131115 (2010).
- 34T. Wilson, N. P. Hylton, Y. Harada, P. Pearce, D. Alonso-Álvarez, A. Mellor, R. D. Richards, J. P. R. David, and N. J. Ekins-Daukes, *Sci. Rep.* **8**, 6457 (2018).
- 35Y. P. Varshni, *Physica* **34**, 149 (1967).
- 36I. Vurgatman, J. R. Meyer, and L. R. Ram-Mohan, *J. Appl. Phys.* **89**, 5815 (2001).